Received: 21 December 2022 | Revised: 26 February 2023 | Accepted: 20 March 2023

DOI: 10.1111/ijac.14431

International Journal of Applied Ceramic Technology

RESEARCH ARTICLE

High aspect ratio sapphire micromachining by ultraviolet laser-induced plasma-assisted ablation (LIPAA)

Douglas F. Cole | **Ricardo J. Zednik** | **Lucas A. Hof**

Department of Mechanical Engineering, École de Technologie Supérieure, Montréal, Quebec, Canada

Correspondence
Lucas A. Hof, Department of Mechanical Engineering, École de Technologie Supérieure, 1100 Notre-Dame Ouest, Montréal, Quebec H3C 1K3, Canada.
Email: lucas.hof@etsmtl.ca

Funding information
Natural Sciences and Engineering Research Council of Canada (NSERC), Grant/Award Numbers: RGPIN-2019-05973, RGPIN-2022-05125; The Mathematics of Information Technology and Complex Systems (Mitacs), Grant/Award Number: IT26841; École de Technologie Supérieure; Edgehog Advanced Technologies Inc.

Abstract

The ultraviolet laser-induced plasma-assisted ablation performed in this article can attain deep and high-quality engravings in sapphire without necessitating volatile solutions or expensive equipment such as high-power ultrashort-pulsed lasers. The dominant mechanism of ablation is discovered to be from the direct ablation of excited sapphire surfaces and not from the plasma generated from the target material. Only an initial deposition from the target is needed to initiate the direct ablation. Note that 20-μm wide, 30-μm deep channel and hole features with a surface roughness (Sa) of .65 μm are achieved at an etching rate of .3 μm per pulse without the need for extensive cleaning. Engravings can reach up to 150-μm depths at a maximum tapering angle of 5° until the shrinking absorbent surface vanishes, and 500-μm wide 430-μm deep topside through-cutting is achieved. This study characterizes the morphology of direct laser ablation of transient absorbent sapphire surfaces. This method demonstrates the potential for the low-cost rapid engraving of high aspect ratio features in transparent sapphire substrates.

KEYWORDS
lasers, manufacturing, morphology, sapphire

1 | INTRODUCTION

Sapphire is an interesting material for emerging Micro-Electro-Mechanical Systems (MEMS), microfluidic and optical devices due to its high strength, hardness, high temperature resistance, and chemical resistance. These applications generally necessitate small feature sizes and a high surface quality. However, current micromachining techniques such as plasma etching and focused ion beam are too slow, expensive, and/or inflexible for accessible rapid prototyping of these emerging devices.[1]

Laser machining offers precision, speed, and low consumable costs, which would make it a promising rapid prototyping technique for sapphire. However, traditional laser-machining requires high energy and ultrashort pulses to directly engrave transparent substrates, which can create cracking.[2] Although expensive, femtosecond lasers can directly ablate sapphire with high precision and can be combined with wet etching to achieve deep high-quality features.[3] The indirect laser machining methods of Laser-Induced Backside Wet Etching (LIBWE)[4] and Laser-Induced Plasma-Assisted Ablation (LIPAA) of var-

ious transparent materials have been studied for over 20 years and show potential for rapid micromachining of sapphire at lower costs than conventional laser machining.[5,6] Through the ablation of an absorbent target material or liquid solution beyond the backside of a transparent material, a laser can create a plasma that can in turn attack the transparent material. Since the threshold fluence of the target is lower than that of the substrate, indirect ablation does not require as much energy as conventional direct laser machining. Although LIBWE has been demonstrated to produce deeper engravings than LIPAA, it requires volatile solutions that make the process hazardous and difficult to prepare.[1]

Lee et al. and Hamdani et al. have achieved 500-μm [5] and 200-μm [7] deep LIPAA scribing of sapphire respectively with Nd:YAG Q-switched lasers. However, the high pulse energy from these lasers results in significant thermal defects. Deep scribing with minimal defects were created by Liu et al. by femtosecond LIPAA [8] and Hanada et al. also demonstrate femtosecond LIPAA coupled with a second laser beam to generate a target plasma.[9] Although good quality engravings can be created by LIPAA, lower power lasers are necessary for accessible sapphire rapid prototyping.

The sapphire engravings produced by LIPAA with lower power lasers have yet to achieve high surface qualities and high aspect ratios, which limits the industrial applicability of these features. Lu et al. have achieved 35-μm wide 20-μm deep engravings[10] and ultraviolet (UV) LIPAA by Sugioka et al. and Li et al both reach 200-nm deep features.[11,12] Other transparent substrates such as fused quartz and Pyrex glass can also be achieved, resulting in .7-mm wide .5-mm deep channel drilling by Zhang et al. with 532- and 1064-nm lasers[6] and micro channels in glass of aspect ratios under 1 by chemical corrosion assisted LIPAA by Pan et al.[13] Hong et al. also demonstrates the use of LIPAA for the metallization of glass backside surfaces and shallow engraving of glass to depths of 6 μm.[14]

LIPAA shows promise for flexible and fast creation of micro channels and holes in sapphire and has the potential for the selective metallization of its features, which could help directly incorporate circuits into microdevices.[15–17] However, the lasers employed for deep feature engraving are either too expensive or produce defects due to high pulse energy. Lower power lasers can process transparent substrates through LIPAA, but micro features machined in sapphire have too low depth or surface quality for most sapphire micro devices. This article analyzes the mechanisms of ablation of low power UV LIPAA sapphire micromachining and investigates the influence of various process parameters on the engraving depth and quality. By closely following the evolution of the engraved features according to the number of pulses delivered, this study uncovers different phases of ablation that present unique micromachining opportunities and challenges. It will also demonstrate the potential of this indirect laser ablation technique for the low-cost rapid prototyping of high quality and high aspect ratio micro features in sapphire.

2 | MATERIALS AND METHODOLOGY

2.1 | Experiment preparation

This study uses a 355-nm DPSS Samurai UV marking system with an average power of 1.5 W, a frequency of 30 kHz, a pulse width of 200 ns and a spot size of 30 μm. Rahman et al. describe an increase in plasma size in function of the fluence[18]; however since the fluence only needs to match the threshold fluence of the target material to generate plasma,[19] and excessive power can induce defects[5], the power was lowered and maintained at .163 W or .1J/cm^2 unless otherwise stated.

Sapphire has a hexagonal crystal structure composed of aluminium (Al^{3+}) and oxygen (O^{2-}) atoms with a and c distances of 4.81Å and 13.12Å, respectively.[20] Although there is an indication that crystal orientation may play a role in nm-scale ablation due to differences in interplanar spacing, no significant effect is found at the micro scale.[21,22] This study uses double side polished 430 μm thick C-plane sapphire substrates which were held at a distance ranging from 0 to 700 μm above the target material where the laser beam was focused. Rahman et al. discuss how the target materials' thermal properties affect the target plasma size and subsequently the size of the engravings on the substrate.[23] Copper, Brass, Silicon, Aluminium 6061-T6, as well as quenched and normalized 1045 and 4140 steel were used as target materials. Roughness and grain size were also taken into account to study the effects of the target material on the substrate engraving.

A schematic process setup is illustrated in Figure 1A, where the sapphire substrate's A-plane and C-plane are indicated. Figure 1B illustrates the hexagonal unit cell of sapphire with the A, C, and M planes and their respective normal directions. The channel features were made in the [010] or [210] directions indicated in Figure 1B. The sapphire was patterned with hole features and channel features with widths varying between 20 and 35 μm. To compare the hole and channel features to each other, an effective number of pulses for channel features was calculated using the frequency (f), spot radius (r), and pass speed (v).

Once the LIPAA is complete, the substrates were cleaned in an ultrasonic bath with hydrochloric acid, acetone, isopropanol and distilled water for 10 min each, and then characterized on a LEXT4100 laser confocal micro-

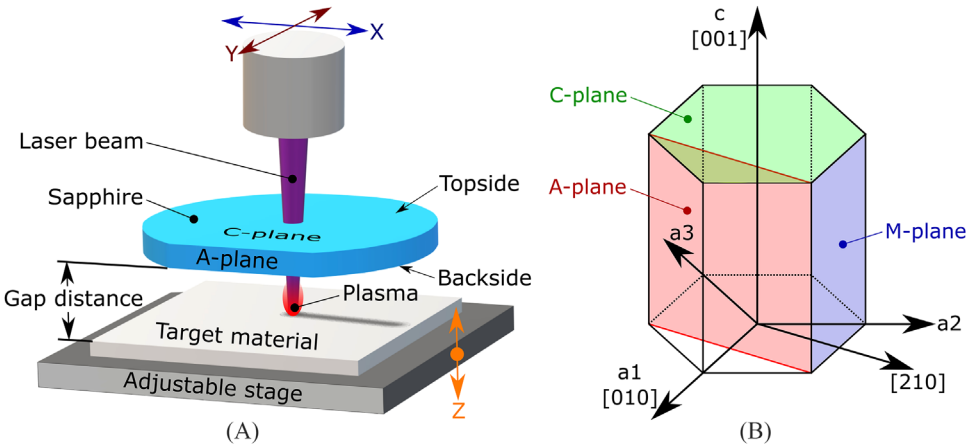

FIGURE 1 Schematic for the (A) laser induced plasma assisted ablation (LIPAA) process setup with sapphire substrate crystal orientation, (B) hexagonal crystal structure of sapphire with A, C, and M planes and their respective normal directions.

scope and a Scanning Electron Microscope (SEM) S3600-N Hitachi with Energy Dispersive X-Ray Analysis (EDX) imaging to study the deposition during the process.

2.2 | Engraving mechanisms

The first ablation mechanism of LIPAA is described as follows. The laser traverses through a transparent substrate and is absorbed by the target material beyond the substrate. This absorption generates a plasma plume, which then attacks the bottom side of the transparent substrate. For the target to ablate, the laser fluence must be above the target material's ablation threshold but below that of the substrate.[24] Certain studies claim that the engraving depth is limited to the size of the plasma.[11,25] As the substrate and target material is consumed, the gap between the two increases and the substrate will be out of reach of the plasma. Beyond the number of pulses required to attain this maximum engraving depth, a deposition of particles from the out-of-reach plasma occurs within the engraved feature. This deposition is said to obstruct subsequent pulses from reaching the target material which further deteriorates the surface quality.[11,25]

The second mechanism is described as follows. The plasma generated from the target material deposits ions on the backside of the substrate. These ions create electron-hole pairs on the backside surface, which enhances the absorption of said surface.[9,26] The laser energy can now be absorbed directly by this surface and ablate the substrate surface simultaneously with the target plasma.[10] In order to study the importance of these mechanisms, the evolution of the depth and the quality of LIPAA engraving is studied in relation to the gap distance, fluence, number of pulses, overlap percentage, frequency, and pulse width.

3 | RESULTS AND DISCUSSION

The evolution of the engraved features between 0 and 2000 pulses was studied for holes and channels. As more pulses are applied to a given area, more ablation takes place, and this results in deeper features. This research discovers distinct phases of sapphire LIPAA resulting from the number of pulses applied, which provide unique challenges and opportunities for micromachining. The quality and depth of hole features produced at low pulse numbers was first investigated to understand the engraving behavior of one-dimensional features.

The channel features demonstrate similar behavior to the hole features but require certain scan speeds to optimize the engraving surface quality. At 75% pulse overlap, 10 passes are required to begin engraving of line features, whereas at 80% overlap, only two passes are required. The greater the overlap between pulses, the more energy is delivered to a given area, and the engraving can take place with fewer passes. However, too much overlap can deteriorate the quality of engraving. The best surface quality of channel engravings was found at a pulse overlap between 75% and 85% (Sa = .65 μm for an area of 20 μm by 250 μm), which corresponds to a speed of 100–150 mm/s or an effective number of pulses per pass of 5.

The evolution of the engraving depth measured by UV confocal microscope before and after the ultrasonic cleaning process as well as the build-up of debris on the target material is shown in Figure 2. The depth of the sapphire channel features before and after cleaning are roughly similar, increasing linearly at a rate of .3 μm per pulse until they

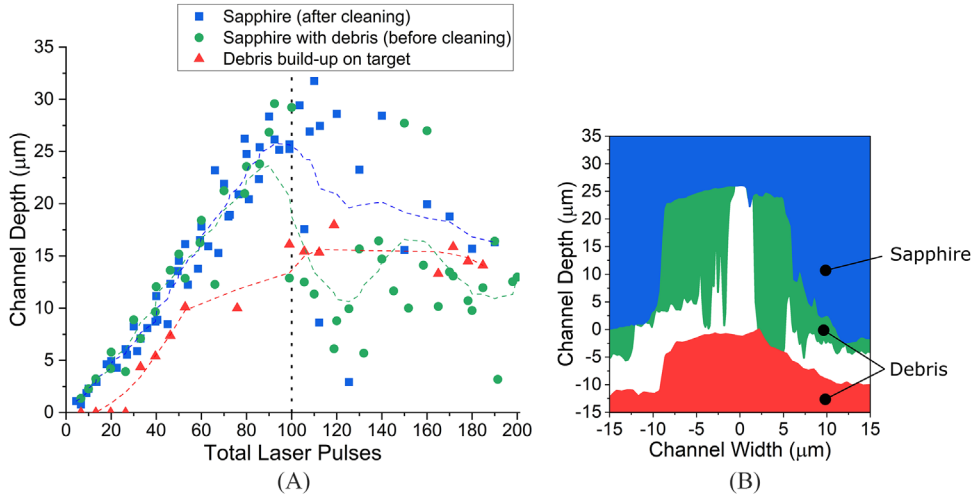

FIGURE 2 LEXT4100 confocal microscope measurements of sapphire engraving depths and debris build-up deposited in sapphire engravings and deposited on the target (A) engraving depth versus the number of effective pulses for 20-µm wide sapphire channel engravings, (B) magnified representative schematic showing sapphire engraving, and debris accumulation at 100 pulses.

reach a depth of around 26 µm at 100 pulses. Beyond 100 pulses, the quality of the engravings deteriorates as is indicated by the sapphire's decreasing moving average dashed lines in Figure 2A.

The ablation of the sapphire propels debris out of the feature and into the surrounding environment. When the gap distance is 0, the debris is trapped between the target and substrate, and the volume of accumulated debris is roughly equal to the volume engraved from the sapphire. The diagram in Figure 2B illustrates the build-up on the target surface (in red) and debris accumulated inside the sapphire feature (in green) when the gap distance is 0. The debris within the feature and on the target material has roughly the same morphology across any number of pulses and has the same combined volume as the ablated sapphire. The debris obstructs the laser from reaching the target material itself, making it impossible for the target to generate a plasma. Since engraving continues nonetheless, the target plasma ablation mechanism can be said to have minimal effect on the engraving, and the ablation must be generated from some other source.

At an approximate aspect ratio of 1, the debris has difficulty fully exiting the channel and will begin to collect on the engraving walls regardless of if there is a gap to provide an escape for debris or not. At 110 pulses, the maximum depth of around 32 µm is reached for both channel and hole features; however the depth and quality of engraving deteriorates beyond 100 pulses, and there is an accumulation of debris within the channel feature. EDX analysis reveals that the debris accumulated within the engraved features and deposited upon the surface of the target material is sapphire. This debris cannot be removed using the ultrasonic cleaning detailed earlier, which suggests that the sapphire debris attaches itself strongly to the sapphire wafer. Further study is required to clean the features at large aspect ratios or to avoid the deposition of debris within channels as the ablation occurs. Apart from the initial deposition, there is no deposition of target material on the backside or within the feature.

To further verify that the saturation in the engraving depth is not from an excess deposition from the out-of-reach target plasma,[11,25] a thin film of a target material can be deposited on the backside of the substrate. By pulsing the target with a low pulse overlap, a deposition of target material on the backside surface of the sapphire can be achieved without ablating the sapphire. By ablating the deposited layer on the substrate without the use of a target under the substrate, the laser cannot generate plasma according to the target plasma ablation mechanism. With an effective pulse per pass of 5, a maximum depth of 32.4 µm was found at 150 pulses before being enveloped by debris. Since there is no significant difference between engraving depths achieved regardless of gap distance, the engraving is not influenced by the target plasma ablation mechanism but rather dominated by direct ablation of a transiently absorptive sapphire surface.[8] This indicates that the newly ablated surface after every pulse retains the ability to absorb the next pulse. The surface remains excited without the need for further action from the target material.

Since the deposited layer on the sapphire is the site for only the initial ablation, all metallic targets enabled engraving with little effect on depth. Since the laser needs this absorbent surface to ablate the sapphire, a uniform thickness and dispersion is desired. Irregular feature shapes were created by normalized steel targets, which

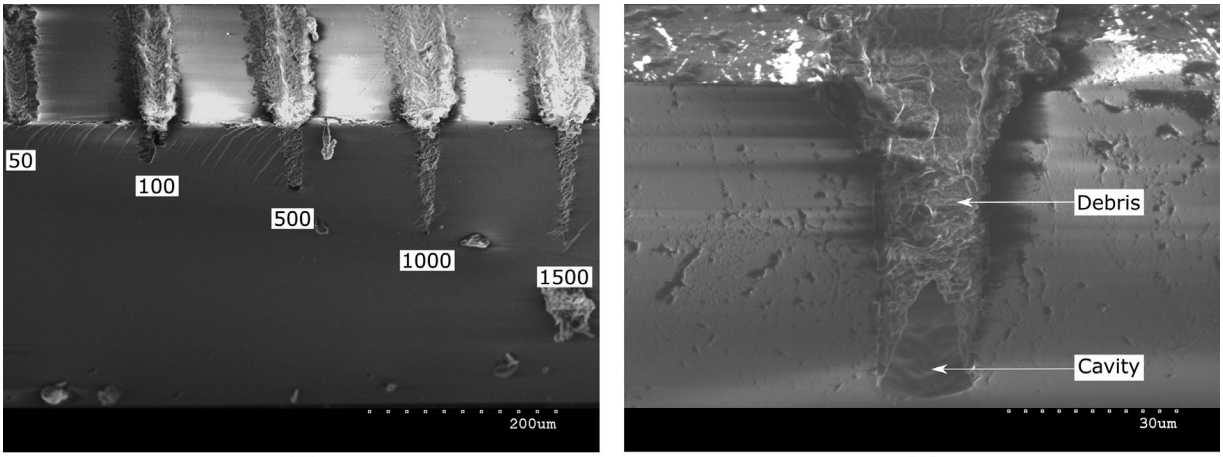

FIGURE 3 45° cross-section SEM image of sapphire (A) engravings at 50, 200, 500, 1000, and 1500 effective pulses, (B) representative image showing cavity and debris accumulation.

may be due to the uneven initial deposition caused by the normalized steels' large grain size (approximately 30 μm in width).

The sapphire was cut parallel to the engravings by scribe and break mechanical separation. The cross-section image shown in Figure 3A reveals that the engraving continues beyond the accumulation of debris. The diagonal cracks seen between the engravings at 50 pulses and 500 pulses are artefacts of the brittle fracture of the sapphire substrate through mechanical cross-sectioning by scribe and break method and are not caused by the laser ablation. Beyond the debris that accumulates at 100 pulses forth, a cavity of air where the latest ablation took place can be found. As more pulses continue to be delivered, the ablation takes place within this cavity, which digs deeper into the substrate, leaving behind more debris. Figure 3B shows that there is a tapering between 2 and 5° of the channel walls as the depth increases, and the channel's absorbent surface shrinks. The engraved surface found in the cavity maintains an approximate surface quality of Sa = .65 μm until around 1000 pulses where at an aspect ratio of 5, the width of the engraving reaches 0 and the cavity vanishes. Varying the power and pulse overlap does not reduce the shrinking of the channel features. The shrinking may be due to the gradual accumulation of debris at the perimeter of the ablated channel surface, which reduces the absorbent surface area for subsequent pulses. The following pulses would then have less and less absorbent surface to ablate. However, without a suitable method for the evacuation of debris during the laser ablation, the source of this shrinkage is unknown.

The saturation of depth measured at 100 pulses by the confocal microscope in Figure 2A is therefore the accumulation of debris of sapphire beginning at an aspect ratio of 1. It does not reflect a limitation for the engraving depth caused by a maximum target plasma height. The engraving rate of .3-μm per pulse continues into this second phase, and if the shrinkage can be avoided, the engraving depth in this phase could theoretically continue much deeper since the ablation source is the sapphire itself.

At approximately 1500 pulses, after the closing of the backside engraving, triangular-shaped features begin to engrave at the topside of the substrate, as seen in Figure 4. The triangular shaped features appear unevenly along the length of a channel feature at first, and then spread along the shape of the engraved feature. When enough pulses have been delivered, the triangular features form approximately 57° angles to the C-plane with widths equivalent to the widths of the engraved features at the backside.

Figure 4A is a 3D height map displaying the morphology of a 30-μm wide backside engraving at 75 pulses, Figure 4B shows the resulting topside engraving that develops with sufficient pulses on the backside 30-μm wide channel. The topside engravings have rough slanted walls (Sa = 3.148 μm) compared to the straight engraving walls of backside engravings. It should be noted that the peaks in the valley of the engraving in Figure 4B represent confocal microscope noise due to excessive measurement depths. The SEM confirms that the depth continues beyond these peaks in reality.

Figure 5A,B shows the triangular features for varying feature sizes and how this topside engraving can create through-cut engraving for 500-μm wide features. The angled walls of these engravings do not absorb the laser directly and their angle and depth does not vary in function of the number of pulses applied beyond 2000 effective pulses. The topside engravings cannot ablate through the debris created from the original backside engravings as seen in Figure 5B. The approximate 57° slope of the triangle features suggests that the removal of sapphire

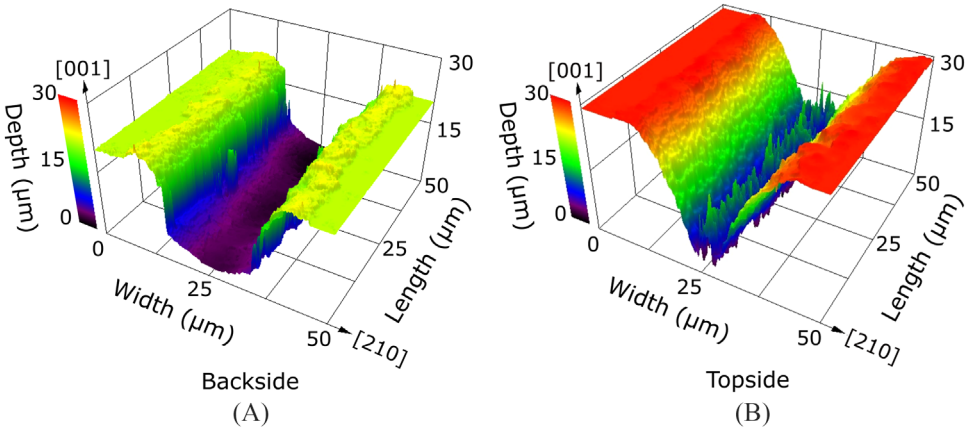

FIGURE 4 Confocal microscope 3D color-height map of sapphire engravings in the A-plane orientation (A) backside engraving for a 30-μm wide feature at 75 effective pulses, (B) topside engraving for a 30-μm wide feature at 2000 effective pulses.

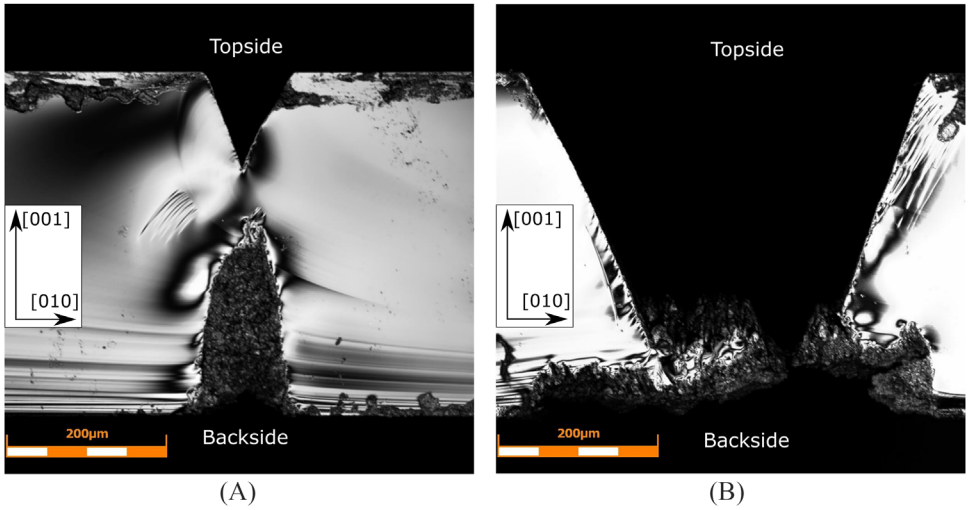

FIGURE 5 Confocal microscope M-plane oriented cross-section images of sapphire engravings (A) 120-μm wide engraving and its resulting topside engraving, (B) 500-μm wide topside through cut engraving.

occurs along the R-plane $\{10\bar{1}2\}$, which has a similar inclination. However, the angles of the topside features do not vary significantly between engravings made in the [010] and [210] directions, which would suggest asymmetry.[27] Further investigation is required to identify the source and ablation mechanism of these topside engravings.

The sapphire UV LIPAA process studied in this research is schematically represented in Figure 6. The ablation of a target material by the first number of pulses renders the backside of the sapphire absorbent to subsequent pulses as revealed by EDX imaging and varying the gap distance. Once the absorbent surface is directly ablated, the engraved surface retains a level of absorbance and can continue to be directly ablated until an aspect ratio of 1, where the debris from the ablated feature sticks to the engraved walls. Although the debris cannot be removed by postprocessing hydrochloric, acetone, isopropanol, and distilled water ultrasonic cleaning, the ablation continues beyond the debris filling until an aspect ratio of 5 is reached, and the feature walls converge. At 2000 pulses, the formation of triangular engravings occurs on the topside of the sapphire.

4 | CONCLUSION

This study identifies three stages of UV laser-induced plasma-assisted ablation of sapphire. The first phase involves the direct ablation of excited sapphire surfaces created from the deposition of an absorbent target material. Only an initial deposition is needed to initiate direct ablation, which can attain 20-μm wide, 35-μm deep channel and hole features with a Sa = .65 μm at a rate of .3-μm per pulse.

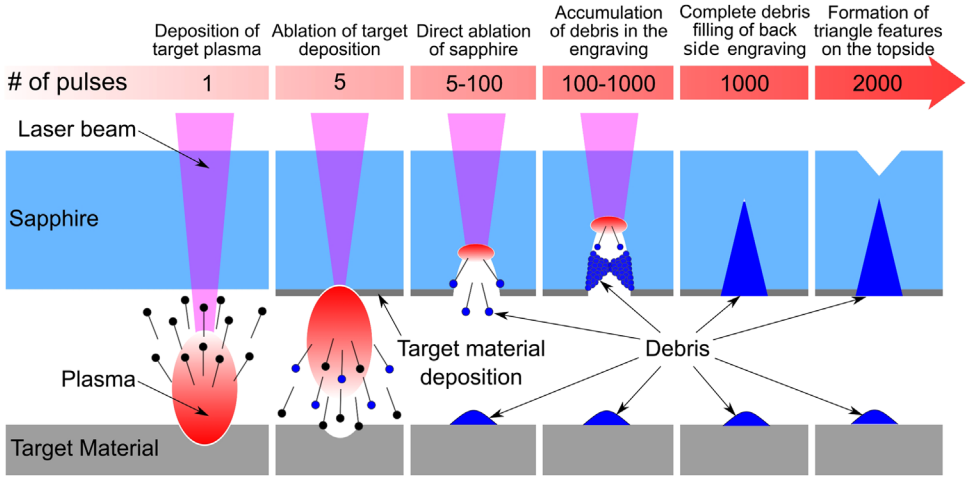

FIGURE 6 Schematic process evolution of laser-induced plasma-assisted ablation (LIPAA) by number of pulses.

The second phase of engraving consists of further direct ablation of the excited feature base, but there is an accumulation of sapphire debris within the engraved feature that must be removed. This phase can reach a depth of around 150 μm with a tapering angle of 5°. The third phase is initiated at the topside surface, where triangle shape engravings forming 57° angles to the C-plane are created. Note that 430-μm deep and 500-μm wide scribing can be achieved in this phase.

Since parallels in ablation mechanisms present themselves in LIBWE, the influence of direct ablation on this process should also be determined. Since only the initial deposition is required for ablation to take place, a cleaning solution could be present at the backside of the sapphire to help remove the debris from the channels as they are ablated. Further investigation on the shrinkage of transient excited surface area is needed to allow for a better understanding of the limiting factors of the depth of the backside direct ablation. We also recommend that further investigation be done regarding the source and ablation mechanism of the topside triangle engravings, and if these features persist even with the evacuation of debris from the backside micromachined features.

The direct ablation of transient absorbent surfaces initiated by UV LIPAA performed in this article can attain 1.5 aspect ratio hole and channel features with high-quality surfaces in sapphire without necessitating volatile solutions or expensive equipment. This process can also achieve through-scribing and has the possibility to create 150-μm deep and 30-μm wide features with the implementation of proper evacuation of sapphire debris. Sapphire micromachining generally requires expensive equipment such as femtosecond lasers; this study demonstrates how indirect laser ablation provides a means for low cost and high aspect ratio rapid prototyping of sapphire.

ACKNOWLEDGMENTS

The authors would like to acknowledge financial support from the Natural Sciences and Engineering Research Council of Canada (NSERC) under the grants RGPIN-2019-05973 and RGPIN-2022-05125, the Mathematics of Information Technology and Complex Systems (Mitacs) under the accelerate grant IT26841, and from École de technologie supérieure under the Programme Impulsion grant. The authors would also like to acknowledge Edgehog Advanced Technologies Inc. for their support and discussion.

ORCID

Douglas F. Cole https://orcid.org/0000-0002-4656-9628

REFERENCES

1. Chen J, Lu X, Wen Q, Jiang F, Lu J, Lei D, et al. Review on laser-induced etching processing technology for transparent hard and brittle materials. The International Journal of Advanced Manufacturing Technology. 2021;117(9):2545–64. Available from: https://link.springer.com/10.1007/s00170-021-07853-2
2. Xia Y, Jing X, Zhang D, Wang F, Jaffery SHI, Li H. A comparative study of direct laser ablation and laser-induced plasma-assisted ablation on glass surface. Infrared Physics & Technology. 2021;115:103737. Available from: https://linkinghub.elsevier.com/retrieve/pii/S1350449521001092
3. Ródenas A, Gu M, Corrielli G, Paiè P, John S, Kar AK, et al. Three-dimensional femtosecond laser nanolithography of crystals. Nat Photonics. 2018;13(2):105–9. Available from: http://www.nature.com/articles/s41566-018-0327-9
4. Cheng JY, Yen MH, Wei CW, Chuang YC, Young TH. Crack-free direct-writing on glass using a low-power UV laser in the manufacture of a microfluidic chip. J Micromech Microeng. 2005;15(6):1147–56. Available from: https://iopscience.iop.org/article/10.1088/0960-1317/15/6/005
5. Lee JM, Jang JH, Yoo TK. Scribing and cutting a blue LED wafer using a Q-switched. Nd:YAG laser. Applied Physics A: Materials

Science & Processing. 2000;70(5):561–4. Available from: http://link.springer.com/10.1007/s003390051080
6. Zhang J, Sugioka K, Midorikawa K. High-quality and high-efficiency machining of glass materials by laser-induced plasma-assisted ablation using conventional nanosecond UV, visible, and infrared lasers. Appl Phys A: Mater Sci Process. 1999;69(7):S879–82. Available from: http://link.springer.com/10.1007/s003390051551
7. Hamdani AH, Nasir A, Sarwar S, Ansar A, Akhter R, Aslam M. Laser etching rates of sapphire glass using metal targets. J Phys Conf Ser. 2013;439:012051. Available from: https://iopscience.iop.org/article/10.1088/1742-6596/439/1/012051
8. Liu H, Li Y, Lin W, Hong M. High-aspect-ratio crack-free microstructures fabrication on sapphire by femtosecond laser ablation. Optics & Laser Technology. 2020;132:106472. Available from: https://linkinghub.elsevier.com/retrieve/pii/S0030399220311051
9. Hanada Y, Sugioka K, Miyamoto I, Midorikawa K. Double-pulse irradiation by laser-induced plasma-assisted ablation (LIPAA) and mechanisms study. Appl Surf Sci. 2005;248(1):276–80. Available from: https://linkinghub.elsevier.com/retrieve/pii/S0169433205004204
10. Lu X, Jiang F, Lei T, Zhou R, Zhang C, Zheng G, et al. Laser-induced-plasma-assisted ablation and metallization on C-plane single crystal sapphire (c-Al2O3). Micromachines. 2017;8(10):300. Available from: https://www.mdpi.com/2072-666X/8/10/300
11. Li Y, Liu H, Hong M. High-quality sapphire microprocessing by dual-beam laser induced plasma assisted ablation. Opt Express. 2020;28(5):6242. Available from: https://opg.optica.org/abstract.cfm?URI=oe-28-5-6242
12. Sugioka K, Obata K, Hong MH, Wu DJ, Wong LL, Lu YF, et al. Hybrid laser processing for microfabrication of glass. Applied Physics A. 2003;77(2):251–7. Available from: http://link.springer.com/10.1007/s00339-003-2116-6
13. Pan C, Chen K, Liu B, Ren L, Wang J, Hu Q, et al. Fabrication of micro-texture channel on glass by laser-induced plasma-assisted ablation and chemical corrosion for microfluidic devices. J Mater Process Technol. 2017;240:314–23. Available from: https://linkinghub.elsevier.com/retrieve/pii/S0924013616303600
14. Hong MH, Sugioka K, Wu DJ, Chew KJ, Lu YF, Midorikawa K, et al. Laser-induced plasma-assisted ablation and its applications. In: Third International Symposium on Laser Precision Microfabrication; 19 February 2003; Osaka, Japan. Available from: http://proceedings.spiedigitallibrary.org/proceeding.aspx?doi=10.1117/12.486532
15. Hanada Y, Sugioka K, Midorikawa K. Laser-induced plasma-assisted ablation (LIPAA): fundamental and industrial applications. In: High-Power Laser Ablation 2006; 7 June 2006; Taos, NM. Available from: http://proceedings.spiedigitallibrary.org/proceeding.aspx?doi=10.1117/12.668667
16. Long J, Li J, Li M, Xie X. Fabrication of robust metallic micropatterns on glass surfaces by selective metallization in laser-induced porous surface structures. Surf Coat Technol. 2019;374:338–44. Available from: https://linkinghub.elsevier.com/retrieve/pii/S0257897219306322
17. Xu S, Liu B, Pan C, Ren L, Tang B, Hu Q, et al. Ultrafast fabrication of micro-channels and graphite patterns on glass by nanosecond laser-induced plasma-assisted ablation (LIPAA) for electrofluidic devices. J Mater Process Technol. 2017;247:204–13. Available from: https://linkinghub.elsevier.com/retrieve/pii/S0924013617301632
18. Rahman TU, Rehman ZU, Ullah S, Qayyum H, Shafique B, Ali R, et al. Laser-induced plasma-assisted ablation (LIPAA) of glass: effects of the laser fluence on plasma parameters and crater morphology. Optics & Laser Technology. 2019;120:105768. Available from: https://linkinghub.elsevier.com/retrieve/pii/S0030399219305778
19. Liu H, Lin W, Hong M. Hybrid laser precision engineering of transparent hard materials: challenges, solutions and applications. Light: Science & Applications. 2021;10(1):162. Available from: https://www.nature.com/articles/s41377-021-00596-5
20. Wen Q, Wei X, Jiang F, Lu J, Xu X. Focused ion beam milling of single-crystal sapphire with A-, C-, and M- orientations. Materials. 2020;13(12):2871. Available from: https://www.mdpi.com/1996-1944/13/12/2871
21. Böhme R, Hirsch D, Zimmer K. Laser etching of transparent materials at a backside surface adsorbed layer. Appl Surf Sci. 2006;252(13):4763–7. Available from: https://linkinghub.elsevier.com/retrieve/pii/S0169433205013759
22. Chen J, Lu X, Li Z, Wen Q, Lu J, Jiang F. Anisotropy of material removal during laser-induced plasma assisted ablation of sapphire. Ceram Int. 2022;48(10):13880–9. Available from: https://linkinghub.elsevier.com/retrieve/pii/S0272884222002899
23. Rahman TU, Qayyum H, Amin U, Ullah S, Rehman ZU, Dogar AH, et al. The role of sacrificial target material in micromachining of glass using laser-induced plasma-assisted ablation (LIPAA). Radiat Eff Defects Solids. 2021;176(7):662–72. Available from: https://www.tandfonline.com/doi/full/10.1080/10420150.2021.1903895
24. Aleknavičien ė I, Pabr ėža E, Talaikis M, Jankunec M, Račiukaitis G. Low-cost SERS substrate featuring laser-ablated amorphous nanostructure. Appl Surf Sci. 2022;571:151248. Available from: https://linkinghub.elsevier.com/retrieve/pii/S0169433221023011
25. Zhao Y, Li Q, Wang Z, Dai Z, Chen T. Microchannel fabrication in fused quartz by backside laser-induced plasma ablation using 248 nm KrF excimer laser. Applied Sciences. 2019;9(24):5320. Available from: https://www.mdpi.com/2076-3417/9/24/5320
26. Hong M, Sugioka K, Lu Y, Midorikawa K, Chong TC. Optical diagnostics in laser-induced plasma-assisted ablation of fused quartz. In: First International Symposium on Laser Precision Microfabrication; 6 November 2000; Omiya, Saitama, Japan. Available from: http://proceedings.spiedigitallibrary.org/proceeding.aspx?articleid=914767
27. Lin J, Jiang F, Wen Q, Wu Y, Lu J, Tian Z, et al. Deformation anisotropy of nano-scratching on C-plane of sapphire: a molecular dynamics study and experiment. Appl Surf Sci. 2021;546:149091. Available from: https://linkinghub.elsevier.com/retrieve/pii/S0169433221001677

How to cite this article: Cole DF, Zednik RJ, Hof LA. High aspect ratio sapphire micromachining by ultraviolet laser-induced plasma-assisted ablation (LIPAA). Int J Appl Ceram Technol. 2023;20:3279–3286. https://doi.org/10.1111/ijac.14431